Hindawi
Geofluids
Volume 2022, Article ID 9962343, 14 pages
https://doi.org/10.1155/2022/9962343

WILEY | Hindawi

Research Article

CO_2 Fluid Flow Patterns near Major Deep Faults: Geochemical and 3D Seismic Data from the Ying-Qiong Basin of the South China Sea

Junfeng Yu,[1,2] **Ruiyou Song**,[2] **Jianxiang Pei**,[2] **Qilin Wu**,[1] **and Yuan Shao**[2]

[1]*Guangdong Research Center for Unconventional Energy Engineering Technology, Guangdong University of Petrochemical Technology, 525000 Maoming Guangdong, China*
[2]*Haikou Company, CNOOC Limited, 570100 Haikou Hainan, China*

Correspondence should be addressed to Junfeng Yu; yujf@gdupt.edu.cn

Received 6 March 2021; Revised 19 September 2021; Accepted 11 February 2022; Published 11 March 2022

Academic Editor: Wei Zhang

Copyright © 2022 Junfeng Yu et al. This is an open access article distributed under the Creative Commons Attribution License, which permits unrestricted use, distribution, and reproduction in any medium, provided the original work is properly cited.

CO_2 and hydrocarbon fluids typically migrate from deeper layers into the shallow crust via large deep faults. Consequently, CO_2, hydrocarbon, and water reservoirs tend to occur in traps near deep and large faults. In this study, we use structural and stratigraphic data to identify and predict CO_2 and hydrocarbon gas reservoirs near major deep faults. In order to investigate how CO_2 accumulates in the major deep faults of the Ying-Qiong Basin (YQB), we quantify the carbon footprint of this area by analyzing the No. 1 fault, the No. 2 fault, and the adjacent gas reservoirs. Using 3D seismic data and geochemical data, we determine how the fault structure affects the ambient CO_2 enrichment on a given fault. Our results indicate that the LD10 and BD19 gas reservoirs have high inorganic CO_2 contents, while the HK29 gas reservoir has a low organic CO_2 content. Based on our analyses, we conclude that the gas source, fault activity, and fault structure control the CO_2 accumulation in subsurface layers. While mantle-derived volcanic inorganic CO_2 disperses upward along the main fault when a given fault is independent (i.e., it lacks secondary faults), the absence of additional vertical migration channels largely prevents the CO_2 from travelling upward through thick mudstone cap rocks and collecting in shallow traps. These shallow traps are typically filled by shallow organic CO_2 sources. However, parallel forward fault-step structures, such as secondary faults, can transport gas that is produced at deeper sources (such as CO_2 generated by basement limestone) to shallower depths. If the hanging wall of a deep fault has many branching secondary faults, then these intersecting faults act as conduits that enable mantle-derived CO_2 to travel vertically into shallow layers.

1. Introduction

CO_2 gas reservoirs mainly form in or near diapir structures, [1–5], deep and large faults [6], the upper strata of volcanic rocks [7–10], and in ultrashallow sedimentary sandstone [11].

One common CO_2 enrichment area is petroliferous basins that are cut by large deep faults [12–16]. Because these large faults can traverse the majority of the lithosphere, they facilitate the formation of CO_2 gas reservoirs via the degassing, rising, and migration of mantle-derived materials [12]. CO_2 reservoirs may also form in traps near large deep faults when carbonate rocks in pre-Cenozoic units decompose at temperatures greater than 550°C [17].

In China, CO_2 gas reservoirs are typically located in the rift basins and continental shelf marginal basins of the Eastern China Sea and the Northern South China Sea [8, 18]. By investigating the development of faults in shallow layers of magma and volcanic rock and collecting borehole drilling data, much work [16, 18, 19] has been done to reduce the risk of CO_2 exploration by determining where CO_2 reservoirs are located along major fault zones. In large deep fault zones, it is possible to make inferences about the type of reservoir(s) (i.e., hydrocarbon and/or a CO_2 reservoir) and the migration channels that are present in the fault zone by analyzing the gas source, the fault activity, and the fault assemblage.

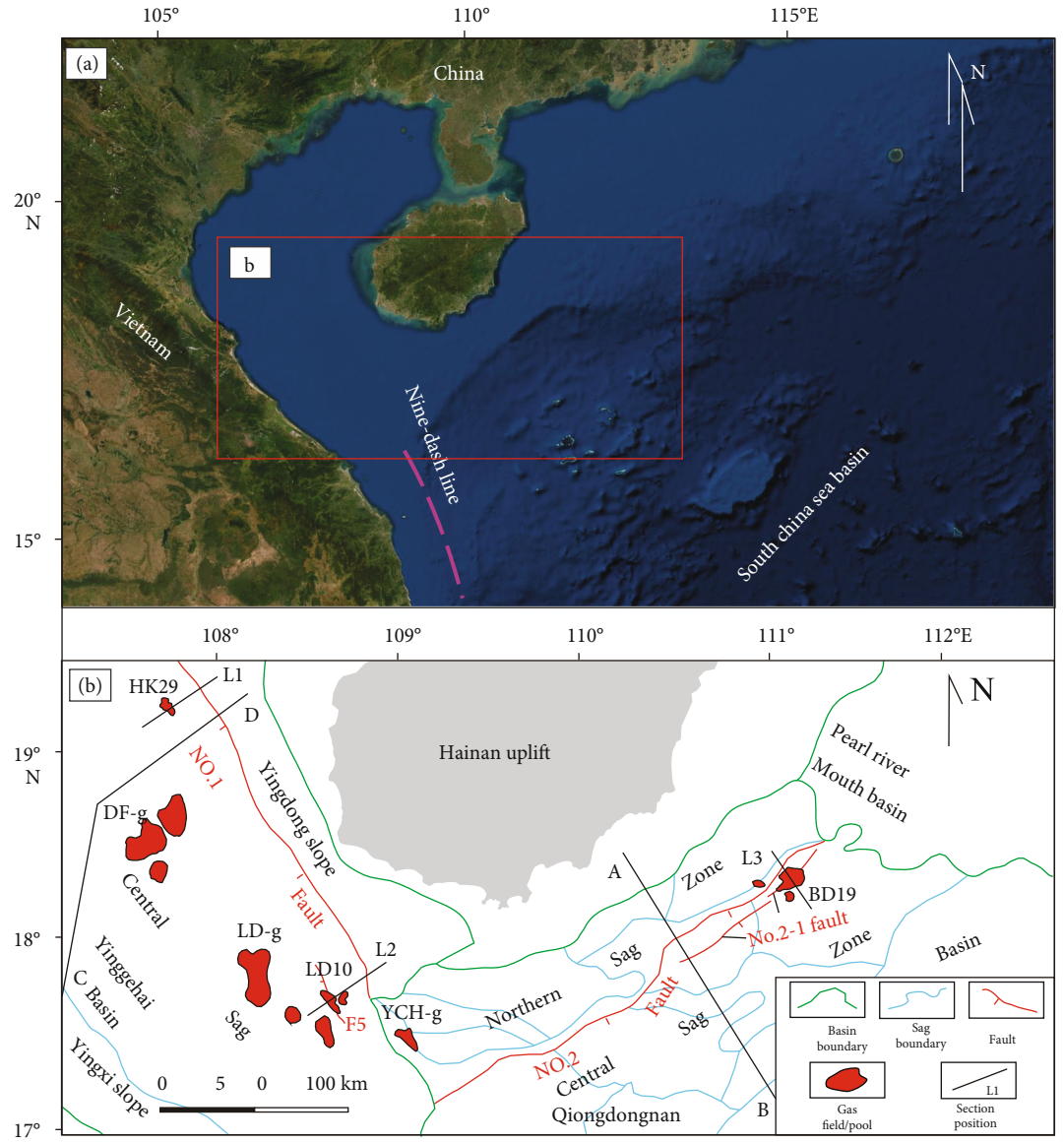

Figure 1: Map of study area. (a) Geographical location of study area. (b) Structural divisions, sections, and gas fields/pools of the Yinggehai and Qiondongnan Basins. DF-g: Dongfang gas reservoir, LD-g: Ledong gas reservoir, YCH-g: Yacheng gas reservoir.

We select two large deep faults in the northwestern South China Sea, the No. 1 fault in the Yinggehai Basin (YGHB), and the No. 2 fault in the Qiongdongnan Basin (QDNB), as our study areas. Several CO_2 gas reservoirs have been discovered along the hanging walls of these fault zones [20–23]. The CO_2 in the BD19 gas reservoir in the eastern part of the No. 2 fault zone originated in the mantle, while the gas in the LD10 gas reservoir in the southern part of the No. 1 fault zone is generated by a mixture of mantle and crustal sources [20, 21, 23, 24].

Despite the progress made in this field, the exact nature of the production and accumulation mechanisms of CO_2 near different deep fault structures is not well constrained. Furthermore, many factors affect these processes, including the possibility of complex gas sources (i.e., mantle source vs. shell source and inorganic vs. organic source), the fault activity history, and the fault structure. To address this uncertainty, we use gas composition data, carbon isotope data, and fault characteristics to determine the CO_2 enrichment of the No. 1 strike-slip in the YGHB and the eastern section of No. 2 fault in the QDNB.

2. Geological Background

2.1. Structural Configuration. The YGHB (area of 11.3×10^4 km^2) is a Cenozoic strike-slip extensional basin located in the passive continental margin of the northwestern South China Sea (Figure 1(a)) [25]. The secondary tectonic units include the Yingdong slope, the Yingxi slope, the Lingao uplift, and the central depression (Figure 1(b)). The No. 1 fault, which is an extension of the Red River fault system, is a large fault that controls the strike-slip movement of the YGHB [26–28]. Previous work indicates that the largest left-hand strike-slip movement on this fault occurred at

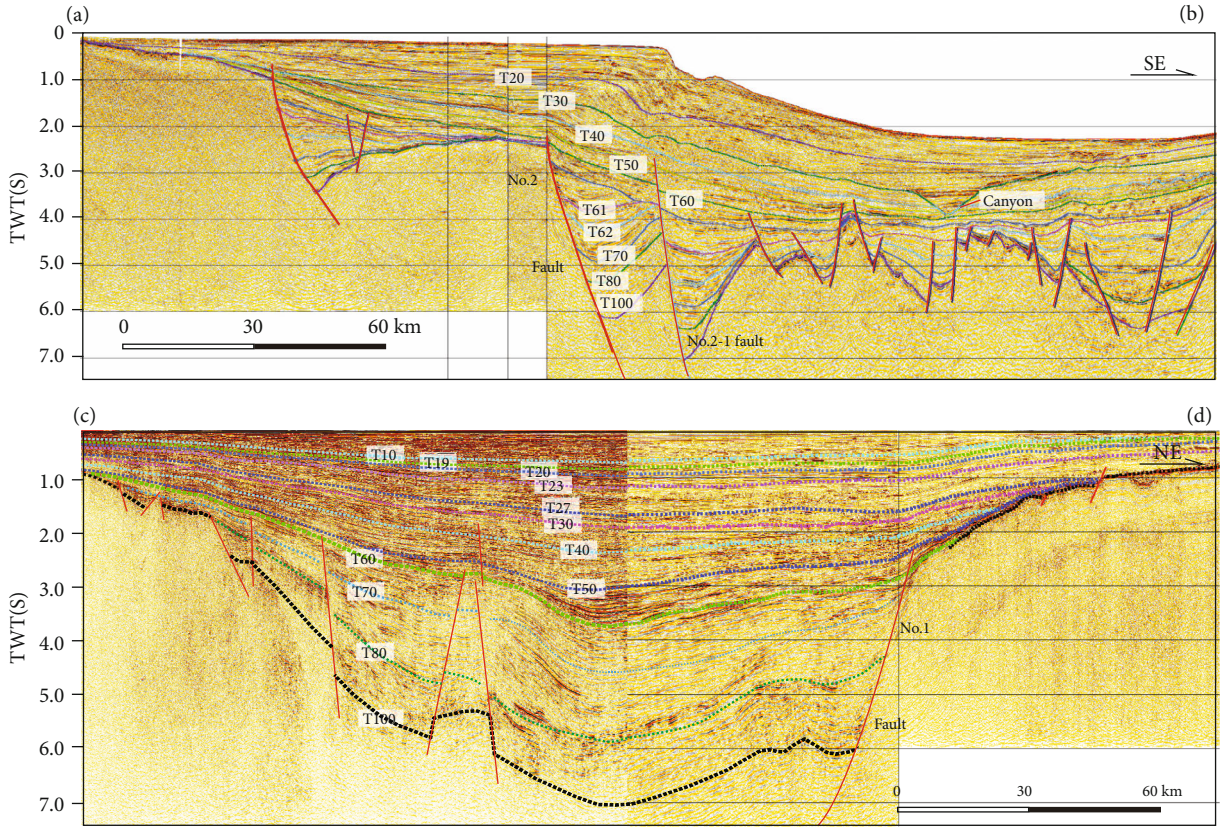

Figure 2: Seismic sections in the Ying-Qiong Basin. Basin locations are shown in Figure 1.

~30–20 Ma. After ~15Ma, this fault transitioned into a right-lateral strike-slip fault; throughout its history, this fault has experienced 500 km of strike-slip motion [26, 29]. From 15 Ma to the present, the No. 1 fault controlled the development of the Yinggehai Sag. A typical half-graben structure formed in the northern part of the YGHB, resulting in the development of a significant fault throw on the hanging wall of the No. 1 fault (Figure 2). Tensile and torsional action near the No. 1 fault created an extensional fault-step structure in the southern part of the basin.

The QDNB is a typical Cenozoic extensional basin that is located next to the YGHB [14]. The main secondary structural units in the basin include the northern depression, the central depression, and the southern uplift [30]. The central depression zone includes five sags (Figure 1(b)): the Ledong Sag, the Lingshui Sag, the Songnan Sag, the Baodao Sag, and the Changchang Sag. The No. 2 fault is a large basement decollement-type normal fault that controls the development of the central depression zone (Figure 2). Its hanging wall is in deep water with a water depth of 1000–2600 m [31]. Due to the growth of the South China Sea block [27, 32], the crust thinned rapidly [33] as the No. 2 fault depression continued to propagate. Gravity and velocity data show that the No. 2 fault extends into the lower crust (Figure 2) [12, 34–36].

2.2. Formation, Source, and Reservoir Cap Assemblages. The YQB contains the complete suite of Cenozoic sediments (Figure 3): Eocene sediments, the Paleogene Yacheng and Lingshui Formations; the Miocene Sanya, Meishan, Huangliu, and Yinggehai Formations; and the corresponding Quaternary and Neogene formations [37]. However, the pre-Cenozoic basement of the YGHB represents the suture between the Indo-China plate and the Eurasian plate. A marine carbonate formation is deposited on the metamorphic basement rock [38]; the CO_2 generated by this carbonate formation has damaged the hydrocarbon gas reservoirs near the diapir s to varying degrees [35, 36]. The two main sets of hydrocarbon source rocks in the YQB are the medium-deep Eocene lacustrine mudstones and the shallow marine calcareous mudstones and siltstones of the Sanya Formation. There are also several sets of reservoir cap assemblages in the Oligocene Lingshui Formation, the Sanya Formation, Member 1 of the Meishan Formation, the Huangliu Formation, the Yinggehai Formation, and the Quaternary Ledong Formation (Figure 3).

2.3. Gas Reservoirs. Eight large- to medium-scale gas fields have been discovered in the Ying-Qiong Basin, with a total proven natural gas reserve of more than 600 billion cubic meters [27, 39–41]. In this study, we discuss the HK29 gas reservoir (in the Sanya Formation), the LD10 gas reservoir (in the Huangliu and Meishan Formations) in the hanging wall of the No. 1 fault, and the BD19 gas reservoir (in the Lingshui Formation) in the hanging wall of the No. 2 fault. These gas reservoirs are excellent natural laboratories in which to study how the main fault zone affects the CO_2 accumulation in these reservoirs.

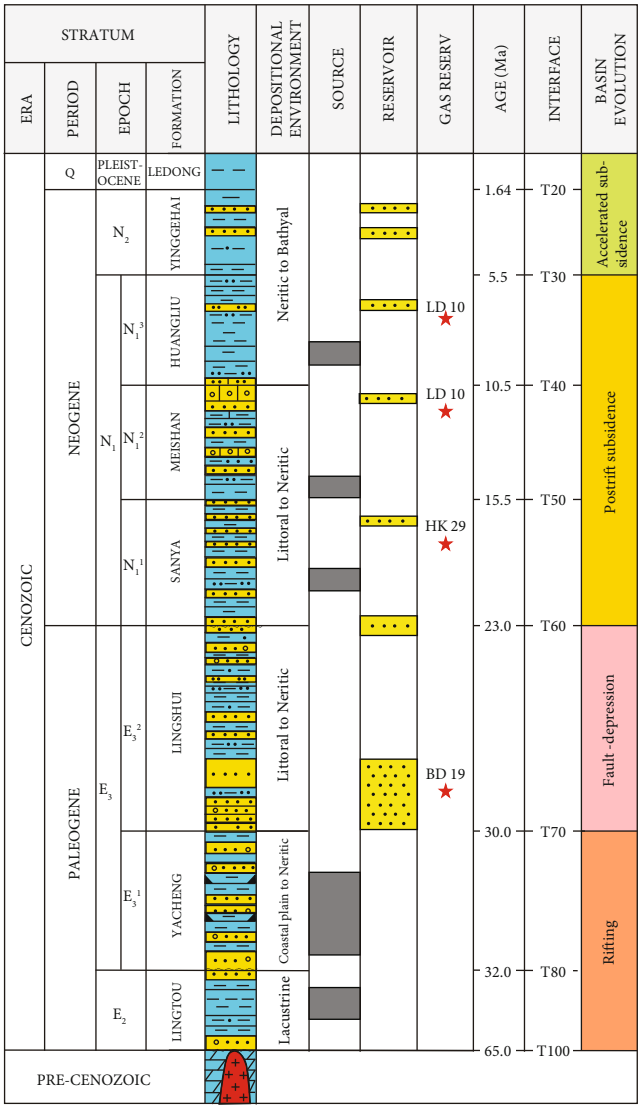

Figure 3: Generalized stratigraphic column of the Yinggehai and Qiongdongnan Basins [21].

3. Data and Methods

Our dataset comprises geochemical data from nine wells and 3D seismic data collected in the Yingdong slope and the Baodao Sag. The geochemical data from three gas reservoirs are shown in Table 1; this geochemical dataset, which includes the three years of drilling data from the LD10 gas field and early drilling data from the HK29 and BD19 gas reservoirs, is a combination of published data [22] and new data.

The gas samples were analyzed using an HP 5890 II gas chromatograph. We conducted stable carbon isotopic analyses similar to those reported by Schoell [42] and Wen and Shen [43] for methane, C_{2+} gaseous hydrocarbons, and CO_2. The $\delta^{13}C$ values are expressed in units of per mil (‰). Based on the PDB standard, our analysis accuracy is ± 0.02‰ [21].

Isotope analyses of the gas samples determined whether the CO_2 source is organic or inorganic in nature. The seismic data provide valuable information about the structure and stratigraphy of the three different gas-bearing tectonic areas. By analyzing both the seismic data and the geochemical data, we determine how the CO_2 accumulation is impacted by the reservoir charging periods, the fault activity, and other tectonic and reservoir features.

We observed and recorded fluid inclusions using a German Leica DM 4500P polarizing and fluorescence microscope; the temperature of these inclusions was measured with a LINKAM THMS-G600 microcooling and heating platform that is controlled by the LINKAM Scientific LINKSYS 32 software package. In our analyses, the temperature was increased or decreased at a rate of 0.1–15 °C/min. Once the inclusion thin slices were polished inclusions, we selected gas–liquid two-phase brine fluid inclusion and organic inclusion samples for homogenization temperature measurements. Typically, more than 15 inclusions were measured in each sample.

The seismic data are displayed in terms of the two-way travel time in seconds. The frequency of the time migrated volume in the Yingdong slope ranges from 10 Hz to 40 Hz, and the estimated vertical resolution for this data is ~15–50 m. The frequency of the time migrated volume in the BD19 reservoir ranges from 20 Hz to 60 Hz, and the estimated vertical resolution for this data is ~10–45 m. Using the GeoFrame software package, we performed the seismic data interpretation, calculated the vertical fault displacements, and determined the relevant fault combination patterns. The fault activity rate (FAR), which reflects the seismic activity intensity in a given area, was calculated using the vertical fault throw. Based on the observation that the stratigraphic sedimentation intervals provide independent constraints on the periods of high fault activity, we conclude that the two basins experienced continuous subsidence without tectonic inversion.

4. Results

4.1. CO_2 Content in Natural Gas. As shown in Table 2, the HK29 gas reservoir located in the northern slope zone of the YGHB mainly consists of hydrocarbon gas, with CO_2 contents of 3.09–8.86% and N_2 contents of 4.08–17.04%. The CO_2 content of the LD10 gas field is less consistent than the values found in the HK29 reservoir; here, the CO_2 content ranges from 0.52% to 62.17%. These CO_2 values are consistent with those of Yang [22]. In the LD10 gas reservoir, the CO_2 content of the Huangliu Formation (0.52–22.43%) is relatively low, while the CO_2 content in the Meishan Formation almost always exceeds 47.36%. As such, the bulk of the CO_2 in the LD10 gas reservoir is produced by the Meishan Formation. Similarly, the CO_2 content of the natural gas in the BD19 gas reservoir exceeds 80%; in this reservoir, a previous study found that that the maximum CO_2 content reached 97.6% [20].

4.2. Isotopic Composition and Origin of the CO_2 Gas. The source of a given CO_2 sample can be identified by examining the carbon isotopic composition. Generally, the degree of light carbon isotope enrichment is greater in organic CO_2

Table 1: Sampling location and characterization of inclusions in the three gas reservoirs.

Gas field	Sample number	Depth/m	Type	Describe
LD10	LD_1010	4238	Saline inclusions containing CO_2	The inclusions are oval in shape and generally 3-9 μm in size. These inclusions are mainly distributed in the fractures of quartz particles, accounting for about 5% of the sample.
HK29	HK29_1	3590	Saline inclusions containing CO_2	It is nearly round, 4-15 μm in size, colorless, and often associated with saline inclusions.
BD19	BD19_220	5155	Gaseous hydrocarbon brine inclusions	Irregular shape, crescent shape, nearly round, and ellipse. They are 2-10 μm in size, and 2-5 μm are mostly small inclusions. The inclusions are mainly gaseous hydrocarbon brine inclusions are 50-60%, with a small amount of CO_2 inclusions.

Table 2: Chemical and carbon isotopic compositions of natural gas generated in three gas reservoirs.

Gas field	Gas pool and sample no.	Formation	Depth/m	Composition of gas/%					Average CO_2%	13°C/‰			Data source
				C1	C2	C3	N2	CO_2		C1	C2	CO_2	
LD10	LD01_11	Huangliu	3982	81.77	2.98	0.6	6.76	7.45	36.6	-32.36	-23.28	-11.83	*Y*
	LD01_51	Huangliu	3995	72.82	1.51	0.12	3.1	22.43		-33.79	-25.88	-1.88	*Y*
	LD02_11	Huangliu	3711	77.71	2.62	0.44	4.87	14.12		-40.71	-27.12	-7.20	*Y*
	LD02_12	Huangliu	3856	85.37	3.9	1.41	7.53	0.52		-34.04	-27.27	-18.08	*Y*
	LD02_13	Meishan	4158	33.08	0.64	0.1	6.99	58.98		-30.8	-23.47	-1.57	*Y*
	LD02_14	Meishan	4062	33.17	0.35	0.04	7.54	58.84		-28.79	-23.78	-2.61	*Y*
	LD03_11	Meishan	4106	47.15	0.11	0.01	5.31	47.36		-28.4	-20.26	-1.10	*Y*
	LD03_12	Meishan	4151	58.88	1.34	0.36	5.59	33.3		-28.67	-22.63	-3.63	*Y*
	LD03_48	Huangliu	4151	44.56	0.11	0.01	3.79	51.42		-28.48	-21.14	-1.52	*N*
	LD13_01	Huangliu	4095-4115	61.64	4.37	1.26	7.45	22.14		-34.11	-21.53	0.71	*N*
	LD13_04	Huangliu	4095-4115	68.72	5.27	1.31	8.16	13.96		-33.67	-20.77	2.60	*N*
	LD13_08	Huangliu	4095-4115	67.65	5.11	1.27	10.3	12.35		-34.34	-21.84	-2.89	*N*
HK29	HK29_1	Sanya	3603.2	73.115	3.204	0.679	15.741	3.094	7.5	-34.42	-21.98	-25.01	*N*
	HK29_2	Sanya	3608-3625	81.28	2.315	0.272	5.54	8.86		-34.42	-21.9	-16.26	*N*
	HK29_3	Sanya	3628.5	78.67	4.94	1.19	4.08	8.6		-37.87	-22.32	-13.67	*N*
BD19	BD19_01	Lingshui	4059.8	1.468	0.042	0.02	8.164	88.772	74.5	-35.7	-21.44	-5.03	*N*
	BD19_18	Lingshui	3388.05	2.242	0.084	2.822		94.267		-42.79	-28.84	-3.85	*N*
	BD19_20	Lingshui		2.607	0.111	0.055		93.757		-43.85	-29.53	-5.06	*N*

Y: cited from reference [22]; *N*: newly added data (for the formation relationship, see Figure 3). LD01, LD02, LD03, and LD13 are all gas pools in the LD10 gas field.

than it is in inorganic CO_2. Additionally, there are noticeable differences in the typical $\delta^{13}C$ values for organic CO_2 (−30‰ to −10‰) and inorganic CO_2 (−8‰ to 3‰) [8, 42–44]. If the $\delta^{13}C$ values fall in the range of −10‰ to −8‰, then the CO_2 has a mixed origin.

Based on these known $\delta^{13}C$ ranges, we conclude that the CO_2 in the HK29 gas reservoir, which has $\delta^{13}C$ values of −25.01‰ to −13.67‰, has an organic origin (Figure 4). The natural gas samples from the Huangliu Formation in the LD10 reservoir (natural gas CO_2 volume of 0.5%–7.5%), which have $CO_2\delta^{13}C$ values of −11.83‰ to −18.08‰, are also generated by an organic source [37] (Figure 4). However, for the LD10 samples with natural gas CO_2 volumes greater than 10%, the $\delta^{13}C$ CO_2 values (−7.20‰ to −0.71‰) indicate that the CO_2 in these samples were generated by an inorganic source (Figure 4).

With $\delta^{13}C$ CO_2 values ranging from −5.06‰ to −3.85‰, we infer that the CO_2 from the Lingshui Formation in the BD19 gas reservoir also has an inorganic source. He et al. [45] suggested that most of the CO_2 near the large deep faults in the QDNB was produced by an inorganic source, while the CO_2 that was found far from the deep faults in the basin was characterized by relatively light CO_2 carbon isotopes that represent a mixed organic-inorganic source.

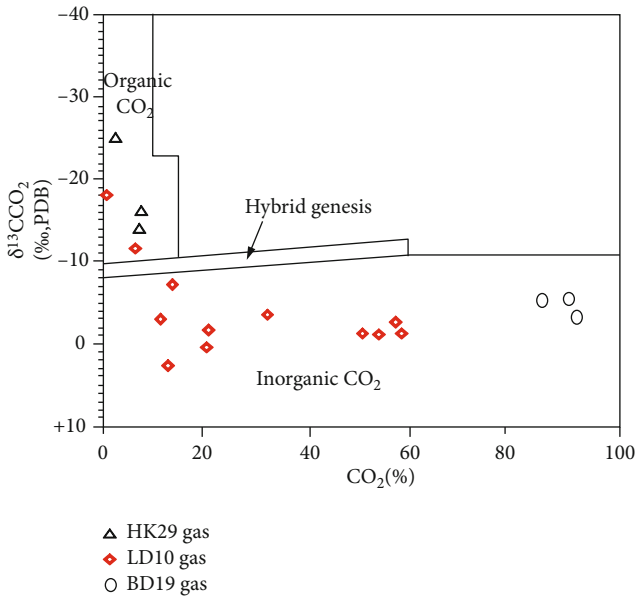

Figure 4: Classification of CO_2 in the HK29, LD10, and BD19 gas reservoirs.

4.3. Filling History of CO_2. Because CO_2 is one of the major volatiles found in geological fluids, the formation of CO_2 reservoirs is somewhat dependent on the nature of the fluids themselves [46]. The CO_2 charging age can be estimated using the homogenization temperature and the burial time of saline inclusions; these saline inclusions act as proxies for CO_2 inclusions in the CO_2 reservoir [47]. As a result, changes in the CO_2 formation homogenization temperatures over time speak to the charging history of those CO_2 samples.

As shown in Figures 5 and 6, the homogenization temperatures of the CO_2 inclusions in the Meishan Formation of the LD10 gas reservoir fall between 150°C and 160°C (Figure 5(a)), which correspond to a burial date/charge date of ~1.2 Ma (Figure 6(a)). A significant amount of hydrocarbon gas was also charged in this time period. The inclusions in the Sanya Formation in the HK29 gas reservoir are relatively developed, with CO_2 inclusion homogenization temperatures that range from 140°C to 150°C (Figure 5(b)). Based on the burial history and the thermal history of the Sanya Formation, we conclude that the charging time was just prior to 2.0 Ma (Figure 6(b)). The homogenization temperatures of the inorganic CO_2 inclusions in the Lingshui Formation sandstone in the BD19 gas reservoir fall in the range of 165°C–190°C, while the hydrocarbon gas homogenization temperatures of the saline inclusions in this unit are slightly cooler (130°C–150°C). These temperatures correspond to a CO_2 gas charge time of 5 Ma and a hydrocarbon gas charge time of 17.5–13 Ma.

4.4. Fault Structures. Faults are important pathways that facilitate fluid flow. As we will demonstrate, the fault structures dictate the pattern of fluid flow near the HK29, LD10, and BD19 gas reservoirs.

4.4.1. Independent Fault Structure. The NE cross-section that samples the HK29 gas reservoir is shown in Figure 7. The most important feature revealed by this cross-section is that the No. 1 fault, as a regional strike-slip fault, cuts into the basement vertically. The No. 1 fault is an independent fault structure; no branch faults have developed in the hanging wall of this large fault zone.

4.4.2. Forward Fault-Step Structure. Unlike the fault structure found near the HK29 gas reservoir, the part of the No. 1 fault that is located close to the LD10 gas reservoir has a forward fault-step structure (Figure 8). At the LD10 reservoir, the No. 1 fault bifurcates, forming two basin-controlled faults that dictate the structure of and the sediment deposition in the hanging wall. In this section of the hanging wall, there are many secondary faults oriented parallel to the main fault; overall, this network of faults creates a forward fault step structure. While our 3D seismic data do not extend past 7S, from the characteristics and age of the No. 1 fault in this location, we infer that the secondary faults extend into the basement material. The secondary faults and the main fault, both of which formed during the initial rifting period, control the development of Paleogene fault blocks in the depression basin.

4.4.3. Branching Fault Structures ("Y" Pattern). As shown in Figure 9, the No. 2 fault system of the BD19 gas reservoir in the QDNB is characterized by many branch faults. The No. 2 fault extends deeply into the basement and controls the development of the hanging wall structure and sedimentation. Here, the secondary branching faults, including the No. 2-1 fault, are all located close to the No. 2 fault.

5. Discussion

The fluid charging mode of a given reservoir is largely dictated by the fluid source, the fault activity, and the fault structural patterns. When filling traps, fluid migrates along the path of least resistance [48], rather than diffusing slowly through low-permeability strata. Because active faults often act as the most efficient pathways for deep fluid migration [49, 50], strong fault activity facilitates fluid movement; when a fault is inactive, fluid flow stagnates.

5.1. The Diverse Origin CO_2 Gas. As summarized in Table 1 and Figure 4, the HK29 gas field contains gas from an organic source. Furthermore, the burial history suggests that the organic CO_2 in this reservoir is likely generated by the pyrolysis of the source rock of in the Sanya Formation. The carbon isotope values of the samples from the LD10 gas field indicate that the gas in this reservoir has a mixed organic-inorganic source. We determined the $^3He/^4He$ ratio of the helium associated with the natural gas that has a high CO_2 content. Because this $^3He/^4He$ ratio (7.78×10^{-8}) is much lower than that of air (1.4×10^{-6}), we conclude that the helium in this reservoir was created by a crustal source [37]. As such, we infer that the large amount of CO_2 in this reservoir was created by the fast thermal decomposition of the deep calcareous mudstones and basement carbonates of the Meishan and Sanya Formations.

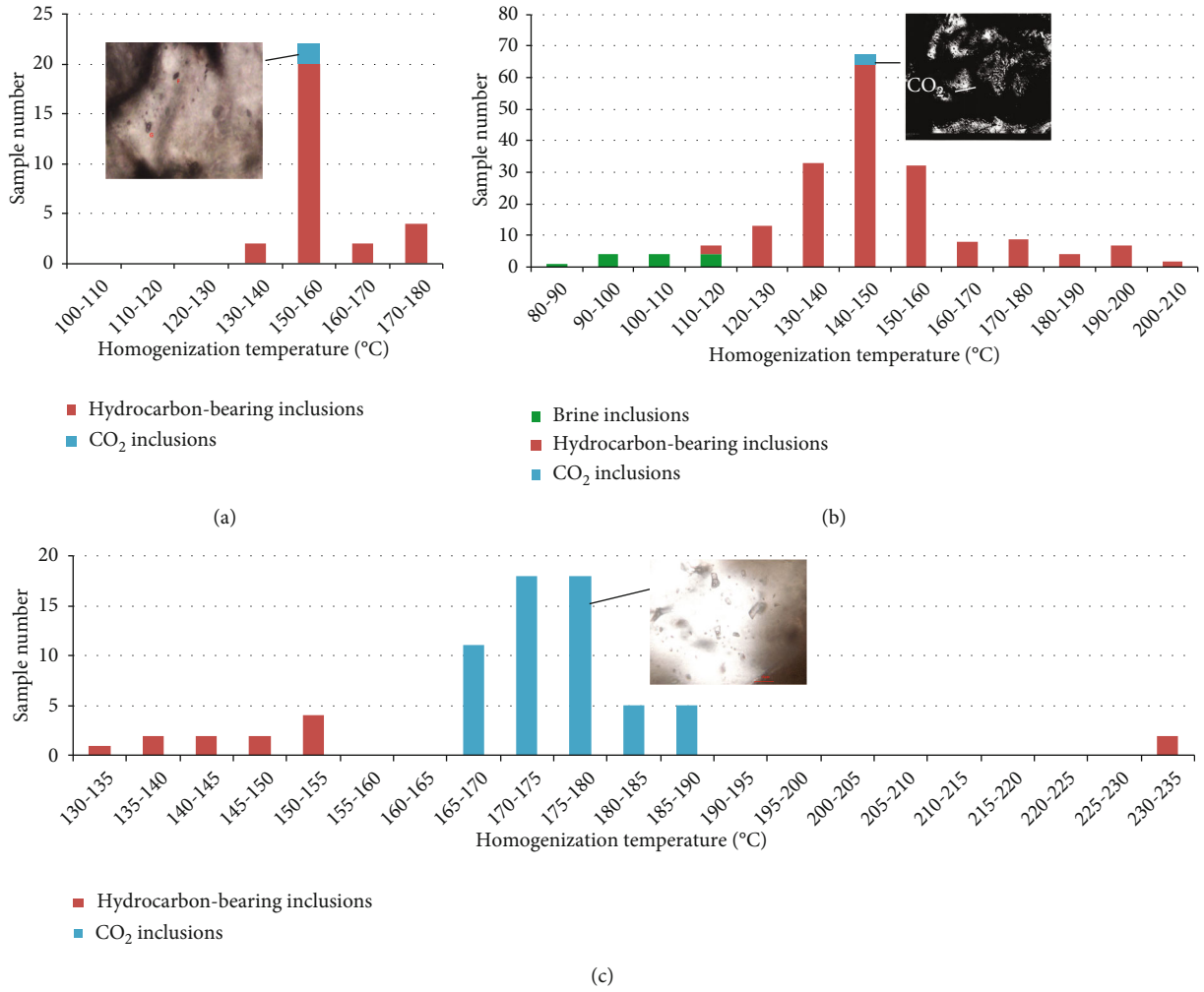

FIGURE 5: Homogenization temperatures of CO_2 inclusions and hydrocarbon inclusions associated with the brine in (a) the LD10 gas reservoir, (b) the HK29 gas reservoir, and (c) the BD19 gas reservoir.

Based on the $^3He/^4He$ values of $34.6 - 87.5 \times 10^{-7}$ and the R/Ra values of 2.47 to 6.25, we infer that the inorganic CO_2 in the BD19 gas field was generated in volcanic mantle material [24, 44]. By analyzing the contact relationships between the volcanic material and the surrounding strata (i.e., the T30 unconformity interface), Xu et al. [23] found that there was volcanic activity in the Baodao Depression in the eastern QDNB at ~5.5 Ma. Because volcanic rocks are not in the geological succession below the CO_2 gas reservoir, it is likely that the CO_2 in this reservoir was initially generated in volcanic magma and was then transported to the trap along the deep fault.

5.2. The Relationship between Fault Activity, Fault Structures, and CO_2 Charging Patterns. Based on the calculated activity rates of the No. 1 fault and the No. 2 fault, we conclude that the most intense fault activity occurred between 32 Ma and 30 Ma (Figure 10); outside of this time period, the fault activity was relatively weak.

With an activity rate of 98 m/Ma on the HK 29 segment of the No. 1 fault at 30–23 Ma, it was possible for deep inorganic CO_2 to still migrate upward along the fault. However, due to a declining fault activity rate (17 m/Ma) during the deposition of the Sanya Formation (23–15.5 Ma), the fluid migration stopped at ~10.5 Ma (Figures 2 and 10). This timing is not consistent with the CO_2 charging time of 2.0 Ma that we estimated using the inclusion homogenization temperature-burial history. This indicates that the deep inorganic CO_2 did not migrate laterally along the fault zone into the HK29 gas reservoir. The HK29 gas reservoir contains organic CO_2 because the Sanya Formation in the YGHB contains calcareous mudstone and calcareous siltstone. These rocks produced hydrocarbon gas and small amounts of organic CO_2 during the mature to highly mature stages. Therefore, some of the organic CO_2 did not originate from a deep source and did not have to migrate far to accumulate into reservoirs in the Sanya Formation sand body.

During the Meishan Formation deposition period (15.5–10.5 Ma), the activity rate of the No. 1 fault near the LD10 gas reservoir was less than 10 m/Ma; by 5.5 Ma, the activity had stopped entirely (Figures 8 and 10). While the F5 fault stopped at 15.5–10.5 Ma, the faults in the overlying strata of the F5 fault continued to be active until 5.5 Ma, which provided a pathway for the vertical migration of deep

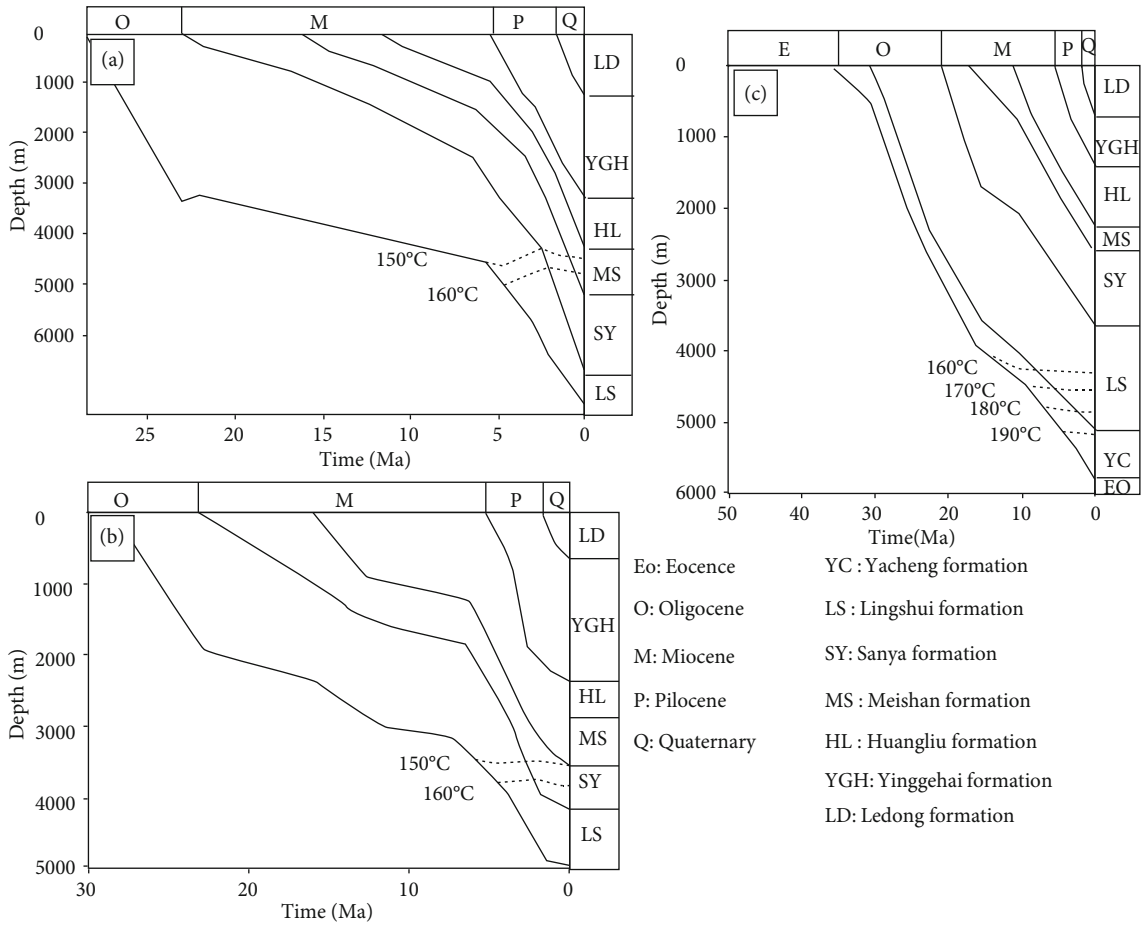

Figure 6: Burial history of (a) the LD10 reservoir, (b) the HK29 reservoir, and (c) the BD19 reservoir in the Ying-Qiong Basin.

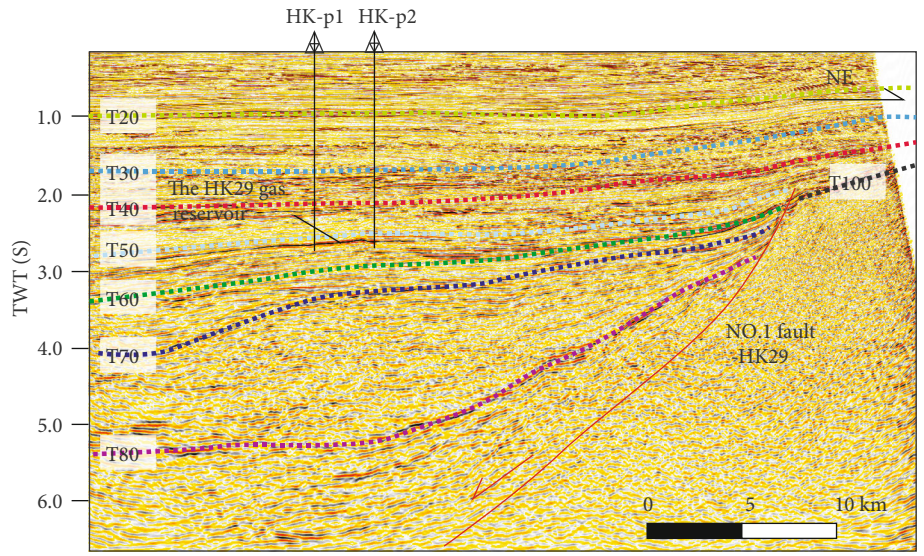

Figure 7: The NE-oriented seismic section (L1) of the HK29 gas reservoir reveals that the No. 1 fault is an independent fault structure that contains no branching faults on the hanging wall. The section location is shown in Figure 1. Our 3D seismic data extend as deep as 7S.

organic and inorganic CO_2 into shallower depths [23]. The results from our inclusion homogenization temperature-burial history projection method indicate that the CO_2 charging time of the LD10 gas reservoir was 1.2 Ma. Previous work by Yang et al. [22] indicates that the inorganic CO_2 formed in the Lingshui Formation at ~15.5 Ma and then

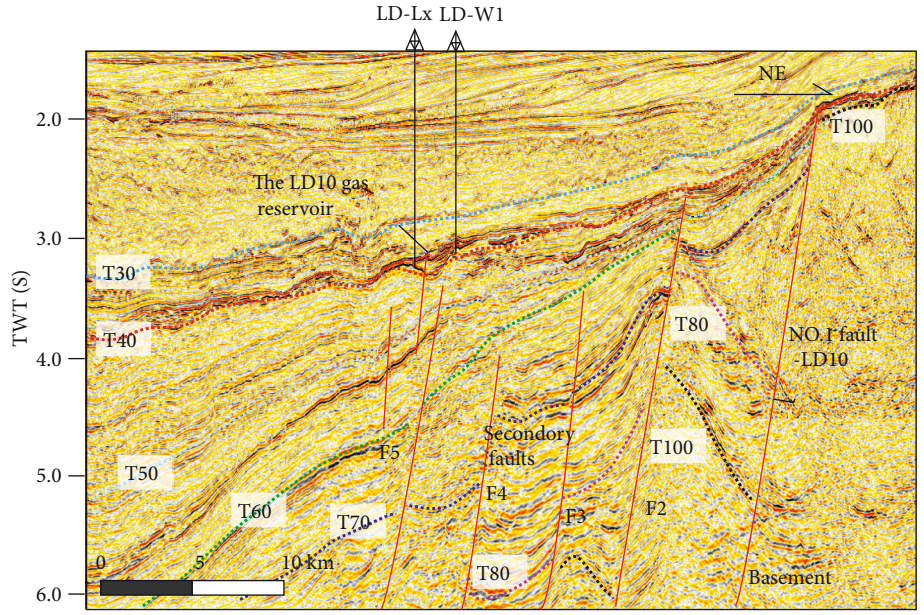

Figure 8: The SE-oriented seismic section (L2) of the LD10 gas reservoir reveals that the No. 1 fault has a forward fault-step structure near the LD10 gas field. The many secondary faults in the hanging wall, which are oriented parallel to the main fault, extend into the basement. The section location is shown in Figure 1. Our 3D seismic data extend as deep as 7S.

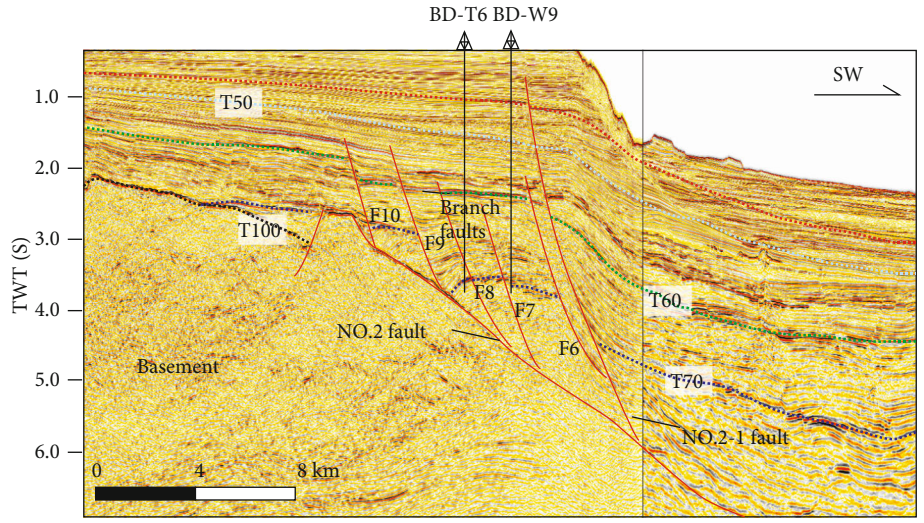

Figure 9: The SW-oriented seismic section (L3) of the BD19 gas reservoir reveals that the No. 2 fault is characterized by a branching structure in the BD19 area. There are many secondary faults in the hanging wall close to the main section of the No. 2 fault. The section location is shown in Figure 1. Our 3D seismic data extend as deep as 7S.

migrated to the traps of the Meishan and Huangliu Formations at 1.2 Ma. The organic CO_2 generated by the Sanya Formation migrated to the same traps, possibly along fluid pathways in opening faults created by overpressure [22].

Unlike the two previous faults, the No. 2 fault activity of the section close to the BD19 gas reservoir stopped at 30 Ma. The No. 2-1 fault was continuously active until the Quaternary (Figure 9). During the deposition of the Lingshui Formation, the fault activity rate was ~90 m/Ma; the activity rate decreased to 2–11 m/Ma between 10.5 Ma and 1.6 Ma. This timeline is consistent with our estimation of the CO_2 charging time of the BD19 gas reservoir via the inclusion homogenization temperature-burial history projection method.

Fault patterns play a significant role in the fluid migration process in general and the vertical migration of mantle-derived CO_2 specifically [16]. The differences in the three fault structures shown in Figures 7–9 affect the CO_2 charging times of the three reservoirs (Figure 11).

Our analysis of the CO_2 contents, carbon isotope values, and tectonic structures of the HK29 gas reservoir indicates that this reservoir contains abundant hydrocarbon gas and a small amount of organic CO_2. We found that this CO_2, which was generated in the Sanya Formation, was

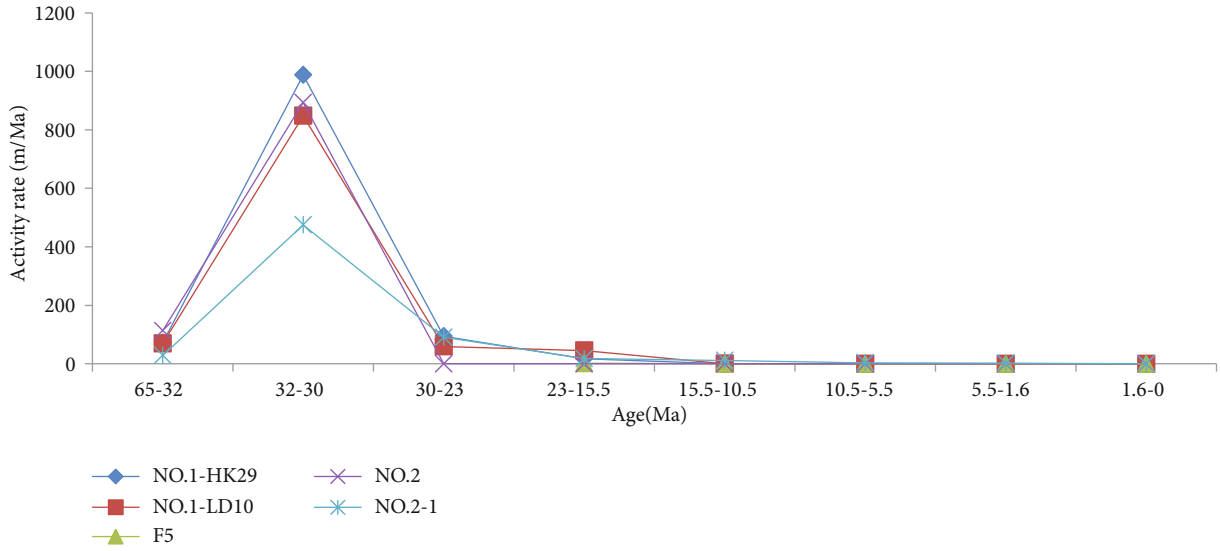

Figure 10: Vertical fault activity rates. Because the T100-T80 interfaces are not included in most of our 3D seismic data, we use the 2D seismic data shown in Figure 2 near the No. 1 and No. 2 faults to calculate the activity rates of the faults during their sedimentary periods. Because fault F5 cannot be identified in the 2D seismic data, we calculate the F5 fault activity rates after 23 Ma using 3D seismic data.

transported directly to the sand body of this layer. Because the basement limestone is overburdened by the thick mudstones of the Eocene and Yacheng formations, the inorganic CO_2 generated by the basement limestones and volcanic activity cannot be transported to the Sanya Formation in the absence of secondary faults. Because the Sanya Formation in this section of the HK29 gas reservoir is inclined upward toward the No. 1 fault (Figure 7), we conclude that the CO_2 migrates upward along the No. 1 fault (Figure 11(a)).

The abundance of mantle-derived inorganic CO_2 in the Lingshui Formation of the BD19 gas reservoir is also related to its fault properties and structure. The many secondary faults on the hanging wall of the No. 2 fault create a "*Y*" shape in the seismic section [16] (Figure 9) that has proven to be an efficient means of facilitating the migration of deep fluids to shallower depths (Figure 11(c)). Hence, branch faults act as secondary conduits for the vertical migration of deeply sourced fluids such as CO_2. Branch faults enhance the fluid delivery capacity of faults; the partial flow caused by these faults also facilitates the horizontal distribution of fluids.

As discussed previously, the LD10 gas reservoir is characterized by a forward fault-step structure that consists of multiple deep basement fault systems (Figure 11(b)). Based on the length scale of the No. 1 fault in this region, we conclude that both main faults and the secondary faults could cut through the whole lower crust in order to enter the deep mantle and the limestone layer in the pre-Cenozoic basement.

5.3. The Possible Gas Seepage in the Vicinity of Large Faults. These three fault structures produce three different gas seepage patterns in the vicinity of the large faults in this area.

The independent No. 1 fault that runs close to the HK29 reservoir became inactive at ~10.5 Ma (Figure 7). As a result, with the exception of the HK29 segment of the No. 1 fault, the deep natural gas cannot migrate through the extremely thick cap rock into shallower reservoirs in most areas of the hanging wall part of the fault; therefore, no fluid leakage occurs here. In the vicinity of HK29 section of the No. 1 fault, however, the leakage pattern in Figure 11(a) shows that a small amount of hydrocarbon gas and a large amount of CO_2, which are generated by processes in pre-Paleogene limestones and the mantle, migrates to shallower depths. The gas phase is not conducive to the formation of high-purity methane hydrate. Moreover, the main fault ceased to be active at about 10.5 Ma; as such, there is no fluid pathway through which the fluid could seep into the seafloor.

The forward fault step structure of the No. 1 fault near the LD10 reservoir produces many secondary faults that are inclined toward the basin and parallel to the strike of the main fault (Figure 8). Above the secondary faults, many local tension fractures that were created by the sinistral strike-slip process formed before 10.5 Ma. These fractures were reactivated and elongated by late stage fluid overpressure. The local tension fractures, which connect to layer-bound faults in shallower strata [51, 52], serve as the primary vertical hydrocarbon seepage paths in the slope area of basin [51].

The ongoing seismic activity experienced by the branching fault structures of the No. 2 fault system near the BD19 reservoir (Figure 9) results in fractures and gas chimneys in the basin; vertically elongated faults or fractures often develop above these earlier faults [53]. Above the gas chimneys, many fractures cut through thin sediment layers. Mass transport deposits (MTDs), which are characterized by low amplitudes, discontinuous and chaotic

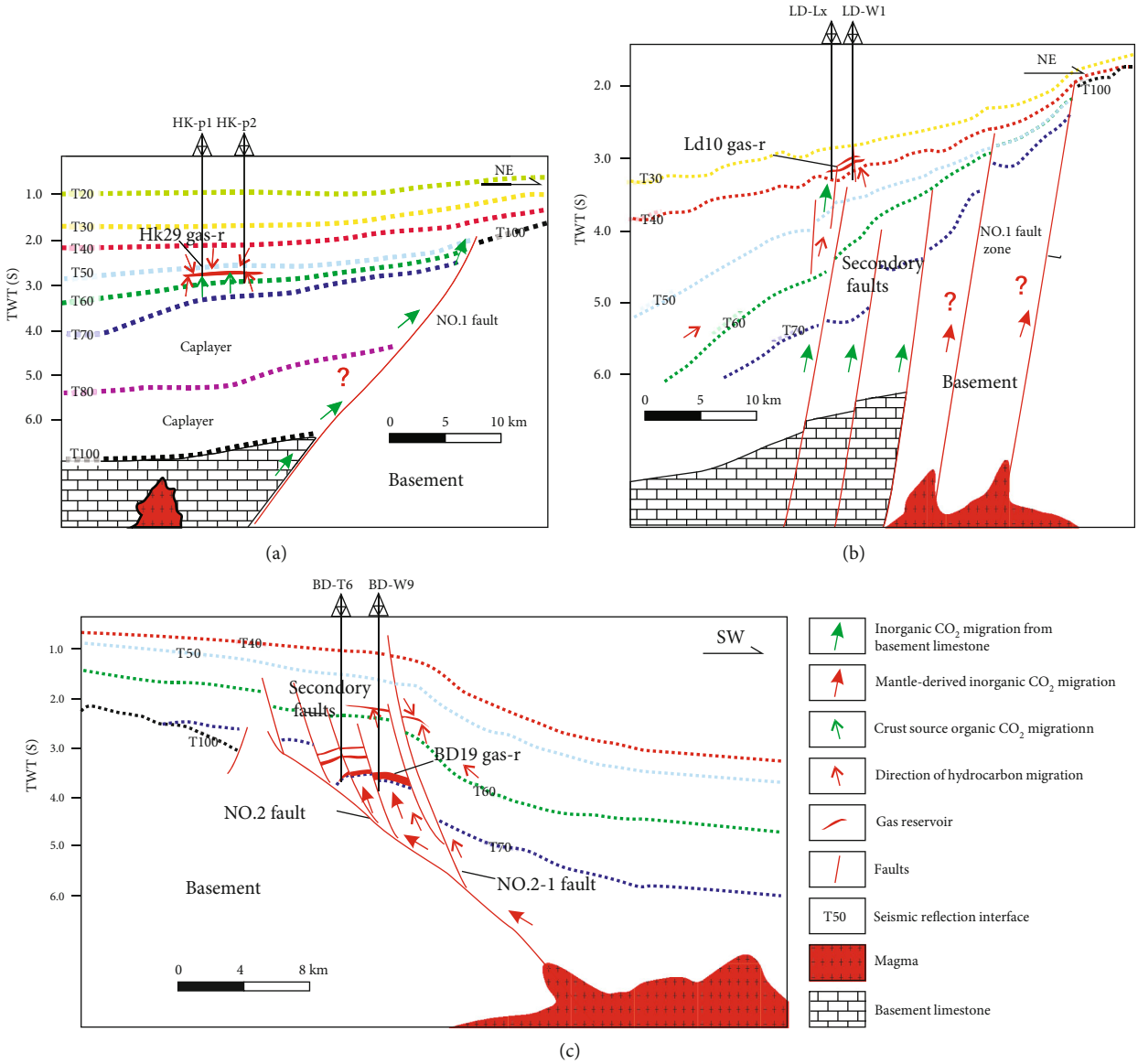

Figure 11: The effect of different fault structures on natural gas charging modes. (a) HK29 gas reservoir formation model. (b) LD10 gas reservoir formation model. (c) BD19 gas reservoir formation model.

reflections, and pockmarks, often develop on the seabed of seepage systems [54]. Between 2016 and 2019, the Guangzhou Marine Geological Survey drilled into the Baodao Sag and collected many hydrate samples [51]. After careful analysis and evaluation of these drilling samples and of additional geological and geophysical data, workers discovered a large hydrate deposit nearby. This work confirmed that the fractures, gas chimneys, deep faults, fault blocks, and buried-hill structures are closely related to gas sources near the BD19 deep fault; overall, these features form a complete leakage system.

6. Conclusions

Based on our work, we have arrived at the following conclusions:

(1) CO_2 fluid migration is active near the No. 1 and No. 2 deep and large faults in the Ying-Qiong Basin. We focused on three CO_2 reservoirs: the HK29 reservoir, the LD10 reservoir, and the BD19 reservoir. These three CO_2 gas reservoirs are quite different from one another. There is very little CO_2 in the HK29 gas reservoir. The organic CO_2 generated by the Sanya Formation fills the trap at approximately 2.0 Ma. The LD10 and BD19 gas reservoirs both have very high CO_2 contents. The LD10 gas reservoir, which contains a mixture of organic and inorganic CO_2, was charged at ~1.2 Ma. The CO_2 in this reservoir is mainly sourced from the thermal decomposition of calcareous mudstones and carbonates in the deep basement. The BD19 gas reservoir, which contains inorganic CO_2 that is derived from volcanic mantle material, charged at ~5.5 Ma

(2) The accumulation of CO_2 in a given reservoir is dictated by the gas source, the fault activity, and the fault structure. In the absence of secondary faults, it is difficult for deep organic CO_2 to migrate vertically through basement limestone covered by thick mudstone cap rock. However, it is possible for inorganic CO_2 to disperse along the main fault; therefore, only shallowly sourced CO_2 can be transported into nearby traps. The forward fault-step structure produces many secondary branching faults that are capable of transporting deep gases, such as CO_2 generated by limestone, to shallow traps. Large deep faults mainly transport the mantle-derived CO_2 upward along the fault. If branching faults have developed on the hanging wall of the main fault, these faults intersect the deep main fault in a "*Y*" shape. The main and branching faults all act as conduits that allow mantle-derived CO_2 to flow vertically into shallow layers

(3) In addition to the three fault structures described throughout this study, there are many faults and stratigraphic combinations that can facilitate fluid flow and the development of hydrocarbon reservoirs. A deeper review of the structural and stratigraphic controls on CO_2 reservoirs will help workers to reduce the exploration risks by successfully predicting the location of hydrocarbon reservoirs

Data Availability

Part of the geochemical data can be downloaded from Elsevier website. The article is named Origin and Migration Model of Natural Gas in L Gas Field, Eastern Slope of Yinggehai Sag, China. The other part of the data can be found in the database of CNOOC Zhanjiang Experimental Center.

Conflicts of Interest

The authors declare that they have no conflicts of interest.

Acknowledgments

This study is financially supported by the Guangdong Research Center for Unconventional Energy Engineering Technology (No. GF2018A011), the Innovation Project of the Educational Commission of the Guangdong Province of China (2020KTSCX084), and the National Key Technology Research and Development Program of China during the "13th Five-Year Plan" (No. 2016ZX05024-002). We are also thankful to CNOOC Ltd., Zhanjiang, for providing us with access to previously published data relating to this topic.

References

[1] E. Pili, Y. Ricard, J. M. Lardeaux, and S. M. F. Sheppard, "Lithospheric shear zones and mantle-crust connections," *Tectonophysics*, vol. 280, no. 1-2, pp. 15–29, 1997.

[2] E. Pili, S. M. F. Sheppard, J. M. Lardeaux, J. E. Martelat, and C. Nicollet, "Fluid flow vs. scale of shear zones in the lower continental crust and the granulite paradox," *Geology*, vol. 25, no. 1, pp. 15–18, 1997.

[3] H. Fang, S. Yongchuan, L. Sitian, and Z. Qiming, "Overpressure retardation of oganic-matter maturation and hydrocarbon generation: a case study from the Yinggehai and Qiongdongnan Basins, offshore South China Sea," *AAPG bulletin*, vol. 29, no. 4, pp. 551–562, 1995.

[4] W. Zhang, J. Q. Liang, P. B. Su et al., "Distribution and characteristics of mud diapirs, gas chimneys, and bottom simulating reflectors associated with hydrocarbon migration and gas hydrate accumulation in theQiongdongnan Basin, northern slope of theSouth China Sea," *Geological Journal*, vol. 54, no. 6, pp. 3556–3573, 2019.

[5] Z. F. Wan, C. M. Chen, J. Q. Liang, W. Zhang, W. Huang, and P. Su, "Hydrochemical characteristics and evolution mode of cold seeps in the Qiongdongnan Basin, South China Sea," *Geofluids*, vol. 2020, Article ID 4578967, 16 pages, 2020.

[6] M. C. Lamberti, N. Vigide, S. Venturi et al., *Structural Control on Carbon Dioxide Diffuse Degassing at the Caviahue-Copahue Volcanic Complex, Argentina*, EGU General Assembly, 2019.

[7] B. Marty, A. Jambon, and Y. Sano, "Helium isotopes and CO_2 in volcanic gases of Japan," *Chemical Geology*, vol. 76, no. 1-2, pp. 25–40, 1989.

[8] J. X. Dai, "Geochemistry and accumulation of carbon dioxide gases in China," *AAPG Bulletin*, vol. 80, no. 10, pp. 1615–1626, 1996.

[9] C. J. Ballentine, M. Schoell, D. Coleman, and B. A. Cain, "Magmatic CO_2 in natural gases in the Permian Basin, West Texas: identifying the regional source and filling history," *Journal of Geochemical Exploration*, vol. 69-70, pp. 59–63, 2000.

[10] Y. M. Liu, Y. Dong, Z. H. Rui, X. S. Lu, X. M. Zhou, and L. C. Wei, "Origin, migration, and accumulation of carbon dioxide in the East Changde Gas Field, Songliao Basin, northeastern China," *Petroleum Science*, vol. 15, no. 4, pp. 695–708, 2018.

[11] D. Schumacher and M. A. Abrams, *Hydrocarbon migration and its near-surface expression*, AAPG Memoir, 1996.

[12] X. L. Qiu, S. Y. Ye, S. M. Wu et al., "Crustal structure across the Xisha Trough, northwestern South China Sea," *Tectonophysics*, vol. 341, no. 1-4, pp. 179–193, 2001.

[13] X. D. Zhang, "Analysis on genesis and accumulation law of carbon dioxide gas reservoirs in the northeastern areas of China," *Acta Geologica Sinica*, vol. 24, no. 6, pp. 13–23, 2003.

[14] J. X. He, B. Xia, D. S. Sun, and S.-L. Zhang, "Hydrocarbon accumulation, migration and play targets in the Qiongdongnan Basin, South China Sea," *Petrolleum Exploration and Development*, vol. 33, no. 1, pp. 53–58, 2006.

[15] E. Roulleau, F. Bravo, D. L. Pinti et al., "Structural controls on fluid circulation at the Caviahue-Copahue Volcanic Complex (CCVC) geothermal area (Chile-Argentina), revealed by soil CO_2 and temperature, self-potential, and helium isotopes," *Journal of Volcanology and Geothermal Research*, vol. 341, pp. 104–118, 2017.

[16] Q. Y. Miao, C. G. Xu, F. Hao et al., "Roles of fault structures on the distribution of mantle-derived CO_2 in the Bohai Bay basin, NE China," *Journal of Asian Earth Sciences*, vol. 197, article 104398, 2020.

[17] H. U. Zhi-Long, H. U. Bao-Jia, G. A. Gang, T. O. Chuan-Xin, and L. I. Jiang-Tao, "Distribution role of CO_2 in shallow gas reservoir and relevant causes in the Yinggehai Basin," *Geoscience*, vol. 24, no. 6, pp. 1140–1147, 2010.

[18] X. Liu, X. Fu, D. Liu et al., "Distribution of mantle-derived CO_2 gas reservoir and its relationship with basement faults in Songliao Basin, China," *Journal of Natural Gas Science & Engineering*, vol. 56, pp. 593–607, 2018.

[19] S. Bigi, S. E. Beaubien, G. Ciotoli et al., "Mantle-derived CO_2 migration along active faults within an extensional basin margin (Fiumicino, Rome, Italy)," *Tectonophysics*, vol. 637, pp. 137–149, 2014.

[20] J. X. He, Y. H. Zhu, X. Huang, and X. F. Gong, "Accumulated mechanisms for different genetic types of non-biological CO2 and controlling factors in north marginal basins, South China Sea," *Natural Gas Geosciences*, vol. 22, no. 6, pp. 935–942, 2011.

[21] B. J. Huang, X. M. Xiao, and X. X. Li, "Geochemistry and origins of natural gases in the Yinggehai and Qiongdongnan basins, offshore South China Sea," *Organic Geochemistry*, vol. 34, no. 7, pp. 1009–1025, 2003.

[22] J. H. Yang and B. J. Huang, "Origin and migration model of natural gas in L gas field, eastern slope of Yinggehai Sag, China," *Petrolum Exploration and Development*, vol. 46, no. 3, pp. 471–481, 2019.

[23] X. D. Xu, Y. Z. Zhang, X. F. Xiong, J. Gan, and G. Liang, "Genesis, accumulation and disribution of CO2 in the Yinggehai-Qiongdongnan Basins, Northern South China Sea," *Marine Geology Frontiers*, vol. 33, no. 7, pp. 45–55, 2017.

[24] N. Liu, K. Q. Wu, L. Liu, L. Yu, and Y. M. Sun, "Dawsonite Characteristics and Its Implications on the CO2 in Yinggehai-Huangliu Formation of Ledong Area,Yinggehai Basin," *Earth Science*, vol. 44, no. 8, pp. 2703–2965, 2019.

[25] J. F. Yu, J. X. Pei, L. F. Wang, J. C. Zhu, and H. Zhang, "Gas pool properties and its exploration implications of the Dongfang 13-2 gravity reservoir-overpressure gas field in Yinggehai Basin," *Acta Petrolei Sinica*, vol. 35, no. 5, pp. 829–838, 2014.

[26] P. Taponnier, G. Peltzer, and R. Armijo, "On the mechanics of the collision between India and Asia," in *Collision Tectonics, Special publication*, M. Croward and A. C. Pand Ries, Eds., no. 19pp. 115–157, Geological Society of London, 1986.

[27] D. E. Hayes, S. S. Nissen, P. Buhl et al., "Throughgoing crustal faults along the northern margin of the South China Sea and their role in crustal extension," *Journal of Geophysical Research*, vol. 100, no. B11, pp. 22435–22446, 1995.

[28] C. K. Morley, "A tectonic model for the tertiary evolution of strike-slip faults and rift basins in SE Asia," *Tectonophysics*, vol. 347, no. 4, pp. 189–215, 2002.

[29] P. Taponnier and G. Peltzer, "Propagating extrusion tectonics in Asia: new insights from simple experiments with plasticine," *Geology*, vol. 10, no. 12, pp. 611–616, 1982.

[30] G.-S. Yao, S.-Q. Yuan, W. Shi-Guo, and C. Zhong, "Double provenance depositional model and exploration prospect in the deep- water area of Qiongdongnan Basin," *Petroleum Exploration and Development*, vol. 35, no. 6, pp. 685–691, 2008.

[31] J. F. Yu, R. Y. Song, C. X. Chao, and G. C. Pan, "Spatial distribution characteristics of fracture system in BSR zone in deep water area of the Qiongdongnan Basin," *Haiyang Xuebao*, vol. 42, no. 9, pp. 69–78, 2020.

[32] T. Y. Lee and L. A. Lawver, "Cenozoic plate reconstruction of Southeast Asia," *Tectonophysics*, vol. 251, no. 1-4, pp. 85–138, 1995.

[33] J. X. He, F. Y. Liu, H. J. Wang, and B. Zhao, "Genetic methanism of deepwter basins and their effects on oil and gas resources on the continental margin of the Northern South China Sea," *Marine Geology Frantiers*, vol. 36, no. 3, pp. 1–11, 2020.

[34] P. Yan, D. Zhou, and Z. S. Liu, "A crustal structure profile across the northern continental margin of the South China Sea," *Tectonophysics*, vol. 338, no. 1, pp. 1–21, 2001.

[35] R. E. Jian-Ye, P. Xiong, L. Chao, Y. U. Li-Zhong, L. I. Jun, and Y. A. Lin-Long, "Ocean and continent transition in passive continental margins and analysis of lithospheric extenstion and breakup process: implication fot research of South China Sea," *Earth Science Frontiers*, vol. 22, no. 1, pp. 102–114, 2015.

[36] J. Ren, X. Pang, P. Yu, C. Lei, and P. Luo, "Characteristics and formation mechanism of deepwater and ultra-deepwater basins in the northern continental margin of the South China Sea," *Chinese Journal of Geophysics*, vol. 61, no. 12, pp. 4901–4920, 2018.

[37] J. H. Yang, X. B. Yang, J. Zhou et al., "Characteristics of inversion structure belts and their hydrocarbon geological significance in the Songnan-Baodao Sag in deep water area of the Qiongdongnan Basin," *Haiyang Xuebao*, vol. 41, no. 5, pp. 97–106, 2019.

[38] B. J. Huang, X. M. Xiao, Z. L. Hu, and P. Yi, "Geochemistry and episodic accumulation of natural gases from the Ledong gas field in the Yinggehai Basin, offshore South China Sea," *Organic Geochemistry*, vol. 36, pp. 1678–1702, 2005.

[39] J. X. He, S. H. Chen, S. S. Cui, W. H. Ma, and X. W. Luan, "Early-stage prediction and evaluation of hydrocarbon source rocks in the deep basin on the northern continental margin of the South China Sea," *Geology in China*, vol. 36, no. 2, pp. 405–416, 2009.

[40] Z. F. Wang and J. X. Pei, "A new accumulation model of high pressure gas in Huangliu formation of the middle-deep interval in Yinggehaibasin: the significance of discovering a good quality gas pay with overpressure and high production in Well DF14," *China Offshore Oil and Gas*, vol. 23, no. 4, pp. 213–217, 2011.

[41] Y. Z. Zhang, X. D. Xu, J. Gan, J. T. Zhu, X. X. Guo, and X. H. He, "Study on the geological characteristics, Accumulation model and exploration direction of the giant deepwater gas field in teh Qiongdongnan Basin," *Acta Peitrolei Sinica*, vol. 29, no. 6, pp. 1–11, 2017.

[42] M. Schoell, "Genetic characterization of natural gases," *Bulletin of American Association of Petroleum Geologists*, vol. 67, pp. 2225–2238, 1983.

[43] Q. B. Wen and Q. X. Shen, "The isotopic composition analysis of organic hydrogen with a steel-tube preparation method," in *Annual Report of Gas Geochemistry Laboratory, Lanzhou Insitute of Geology*, Science Press, Beijing, 1991.

[44] M. Schoell, P. D. Jenden, M. A. Beeunas, and D. D. Coleman, "Isotope analysis of gases in gas field and gas stroage operations," *Jawro Journal of the American Water Resources Association*, vol. 14, no. 14, pp. 384–393, 1993.

[45] J. X. He, B. Xia, and D. S. Sun, "Hydrocarbon accumulation, migration and play targets in the Qiongdongnan Basin , South China Sea," *Petrolleum exploration and development*, vol. 3, no. 1, pp. 53–58, 2006.

[46] M. A. Kokh, N. N. Akinfiev, G. S. Pokrovski, S. Salvi, and D. Guillaume, "The role of carbon dioxide in the transport and fractionation of metals by geological fluids," *Geochimica et Cosmochimica Acta*, vol. 197, pp. 433–466, 2017.

[47] C. Honghan, M. Lijun, L. Yanhua, H. Jinyang, and K. Lingtao, "Genesis, distribution and risk belt prediction of CO_2 in deep-water area in the Pearl River Mouth Basin," *Acta Petrolei Sinica*, vol. 38, no. 2, pp. 119–133, 2017.

[48] P. Xiongqi, J. Zhenxue, H. Handong, C. Dongxia, and J. Fujie, "Formation mechanisms, distribution models, and prediction of superimposed, continuous hydrocarbon reservoirs," *Acta Petrolei Sinica*, vol. 5, pp. 795–828, 2014.

[49] R. J. Knipe, "The influence of fault zone processes and diagenesis on fluid flow, in Horbury, A.D. and Robinson, A.G., (Eds.), Diagenesis and basin development," *AAPG Studies in Geology*, vol. 36, pp. 135–151, 1993.

[50] S. R. Hibson, "Fluid involvement in normal faulting," *Journal of Geodynamics*, vol. 29, no. 3-5, pp. 469–499, 2000.

[51] C. W. Fan, "Tectonic deformation features and petroleum geological significance in Yinggehai large strike-slip basin, South China Sea," *Petroleum Exploration and Development*, vol. 45, no. 2, pp. 204–214, 2018.

[52] C. Lei, J. Ren, P. D. Clift, Z. Wang, X. Li, and C. Tong, "The structure and formation of diapirs in the Yinggehai-Song Hong Basin, South China Sea," *Marine and Petroleum Geology*, vol. 28, no. 5, pp. 980–991, 2011.

[53] N. Baristeas, Z. Anka, R. di Primio, J. F. Rodriguez, D. Marchal, and F. Dominguez, "Distribution of hydrocarbon leakage indicators in the Malvinas Basin, offshore Argentine continental margin," *Marine Geology*, vol. 332-334, pp. 56–74, 2012.

[54] J. Q. Liang, W. Zhang, J. A. Lu, J. Wei, Z. Kuang, and Y. He, "Geological occurrence and accumulation mechanism of natural gas hydrates in the eastern Qiongdongnan Basin of the South China Sea: Insights from site GMGS5-W9-2018," *Marine Geology*, vol. 418, p. 106042, 2019.